IET Microwaves, Antennas & Propagation

WILEY

The Institution of Engineering and Technology

ORIGINAL RESEARCH OPEN ACCESS

Compact Planar Zero-Ground-Clearance End-Fire CP Antenna With Integrated Slow-Wave Structure for Mobile Terminal Applications

Huacheng Li[1] | Wei Lin[1] | Chow-Yen-Desmond Sim[2]

[1]Department of Electrical and Electronic Engineering, The Hong Kong Polytechnic University, Hong Kong SAR, China | [2]Department of Electrical Engineering, Feng Chia University, Taichung, Taiwan

Correspondence: Wei Lin (w.lin@polyu.edu.hk)

Received: 23 December 2024 | **Revised:** 27 February 2025 | **Accepted:** 18 March 2025

Handling Editor: Wen-Jiao Liao

Funding: This work was supported by the Research Grants Council of Hong Kong, SAR, China, under Project PolyU 25213623 and Project AoE/E-101/23-N.

Keywords: antennas | mobile satellite communication | substrate integrated waveguides

ABSTRACT

This paper introduces a novel compact planar end-fire antenna system featuring circularly polarised (CP) radiation and zero ground clearance. The system is constructed using a half-wavelength $TE_{0.5,0}$ mode open waveguide, which inherently generates vertically polarised electric components. By incorporating a slow-wave (SW) structure in the form of metallised blind via holes within the waveguide, a significant SW effect is achieved, resulting in a 40% reduction in the waveguide longitudinal size compared to the conventional counterpart design. Furthermore, by etching an open-ended slot in the top metallic surface of the waveguide, the edges of its aperture are enabled to generate an electric dipole mode. In this way, the horizontally polarised electric components can be achieved without increasing the antenna's footprint. With the proper combination, the design can effectively achieve the required 90°-phase difference in the end-fire direction for these two components. Finally, a 2.5 GHz antenna was designed and optimised. Aiming to mimic the practical environment of mobile terminal devices, a large metallic ground was adopted under the antenna in the simulation and experiment. The measured results indicated that an overlapped impedance $|S_{11}| < -10$ and axial ratio (AR < 3) bandwidth of 2.7% from 2.495 to 2.562 GHz is achieved. The proposed antenna shows great potential in wireless communication applications for mobile terminal devices.

1 | Introduction

Planar end-fire antennas (the maximum radiation beam is pointing to the direction that is in parallel with the surface of the planar antenna) are attractive for wireless communication applications due to their favourable features such as compact size, low profile, lightweight and ease of integration, etc. [1]. In particular, planar end-fire circularly polarised (PECP) antennas have received much attention recently because of their ability to avoid polarisation mismatch problems that arise from linearly polarised (LP) systems [2]. For instance, in satellite communications [3] and mobile terminal device applications [4, 5], etc.

Much effort has been made to develop PECP antennas to date [6–17]. They can be simply summarised into four categories. The first type is to use the turnstile structure, like a helical antenna in Chen and Shen [6]. The second one is to use travelling-wave methods, such as the offset parallel strip structure [7]. The third way to generate CP radiation is by introducing a sloping slot as a polariser [8]. Additionally, the most

popular one is to combine two radiators with orthogonal polarisations. The phase difference between these two radiators can be provided by introducing compensation lines [9–13], etching slots [14, 15], or special compensation structure [16, 17] and then the CP wave is synthesised. In general, cavities acting as a magnetic dipole to provide vertical polarisation are commonly employed. Then, different horizontally polarised radiator types will be utilised for CP radiation. For instance, the designs in Lu et al. [9] incorporate a cavity and a loop radiator. The designs in Ye et al. [13] adopt printed dipole radiator and cavity. In Guo [14], a design combines the coupled-mode patch antenna (CMPA) and crossed ground slot radiators to generate the CP radiation. Although the research works have been presented with excellent performance, in practical mobile devices, most designs require a large unobstructed area to be reserved on the metallic ground to ensure that the antenna works properly, as shown in Figure 1.

However, it should be emphasised that, as wireless communication systems continue to evolve, there is an increasing demand for compact terminal devices. This trend towards miniaturisation necessitates those antennas should be as compact as possible. More critically, the clearance area of the antenna should be further minimised to enable seamless integration with the printed circuit boards (PCBs) used in these devices. Antennas with zero ground clearance are particularly promising [18].

However, designing an end-fire circularly polarised (CP) cavity antenna that achieves both zero ground clearance and a compact size presents significant challenges due to profile limitations. The study in Sun and Wang [15] demonstrates a CP antenna with zero ground clearance that is achieved by etching a slot in the top surface of an open waveguide. Although this configuration achieves CP end-fire radiation with zero ground clearance, it necessitates an auxiliary LC impedance-matching network to optimise port reflection characteristics. Furthermore, the design exhibits a limited end-fire gain of 0 dBic and restricted 3 dB axial ratio (AR) beamwidths (< 45° in the *yoz*-plane).

In this work, we propose a compact planar end-fire CP antenna that features zero ground clearance and a simple structure. The approach is to combine the SW-loaded $\lambda/2$ $TE_{0.5,0}$ mode open waveguide and open-end slot. The open waveguide acts as a magnetic dipole with vertical polarisation. The horizontally polarised components are provided by the electric dipole mode, which is realised by etching an open-ended slot in the top metallic surface of the waveguide. By properly tuning the length and position of the slot, the requirement of phase and amplitude for the CP radiation can be realised. Subsequently, to reduce the longitudinal size of the antenna, an effective method involving the integration of SW structure into the waveguide is employed, achieving a 40% reduction in size. Finally, to validate the effectiveness of our design idea, a 2.5 GHz CP end-fire antenna (covering the S-band of the BeiDou Navigation Satellite System of 2483.5–2500 MHz) is designed on a 70 mm × 140 mm ground plane. The ground clearance is defined as the clean area reserved on the ground plane for the antennas, and in this design, the clearance is 0 mm. A prototype of the antenna was fabricated by PCB manufacturing technologies. It is very simple and easy to integrate with the PCB.

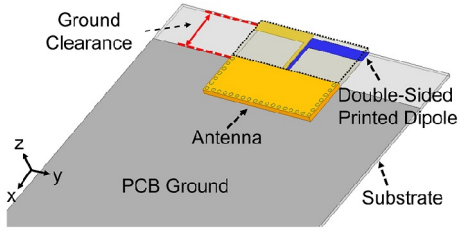

FIGURE 1 | Conceptual illustration of the typical planar end-fire CP antenna with a large clearance area.

2 | Antenna Design and Operating Principle

In this section, the development of an end-fire CP design is present, which is derived from a half-mode open waveguide with an integrated SW structure. Its operating principles are explored through parameter studies conducted using full-wave simulation.

2.1 | Antenna Configuration

The geometry of the proposed compact planar zero-ground-clearance end-fire CP antenna with integrated SW structure is shown in Figure 2. The entire design is very concise and is

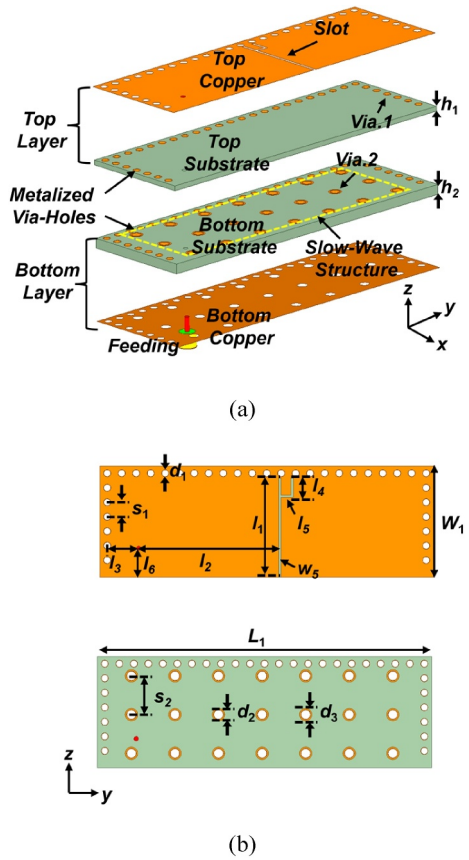

FIGURE 2 | Geometry of the proposed compact planar zero-ground-clearance end-fire CP antenna. (a) Exploded view and (b) top view of the top copper and top view without top layer.

constructed by a two-layer stacked PCB: Top Substrate and Bottom Substrate as shown in Figure 2a. The two substrates are both F4BM, having a dielectric constant (ε_r) of 2.2 and a loss tangent (tanδ) of 0.001. The thickness of the top and bottom substrate is h_1 and h_2, respectively. The thickness of printed copper metal surfaces is 0.5oz each. These two layers are closely bound by metal screws. Besides, there are two kinds of metallic via holes. Via.1 with diameter d_1 is a set of metallised via holes, which are connected between Top Copper and Bottom Copper. They are used to form the sidewall of the $TE_{0.5,0}$ mode open waveguide. Whereas metallised blind via holes (Via.2) with a small ring at the top have a diameter of d_2 and centre-to-centre spacing between two adjacent vias s_2, which are connected to Bottom Copper only to realise the SW structure. In addition, a fork-like open-ended slot is etched into the top metallic surface of the waveguide as shown in Figure 2b.

All the corresponding design parameters have been optimised by Ansys HFSS and are listed as follows:

$h_1 = 1$ mm, $h_2 = 2$ mm, $W_1 = 23$ mm, $L_1 = 69$ mm, $d_1 = 1.5$ mm, $d_2 = 2$ mm, $d_3 = 2.6$ mm, $s_1 = 3$ mm, $s_2 = 9$ mm, $l_1 = 20.5$ mm, $l_2 = 29$ mm, $l_3 = 6.5$ mm, $l_4 = 4$ mm, $l_5 = 2$ mm, $l_6 = 6$ mm, $w_5 = 0.5$ mm.

2.2 | SW-$TE_{0.5,0}$ Mode Open Waveguide

The proposed design is based on a conventional half-wavelength $TE_{0.5,0}$ mode open waveguide operating at 2.5 GHz as depicted in Figure 3a. Since the fundamental design principles have been thoroughly discussed in previous studies, they are not reiterated here to avoid redundancy [19]. In many mobile applications, reducing the transverse dimensions (W_1) of antennas is essential to meet the large screen requirements of current devices. Therefore, to validate the effectiveness of the SW structure, we developed a waveguide with a reduced transverse size (W_1) as a proof of concept. This waveguide has a total width of 23 mm (0.19 λ_0) and a length of 109 mm (0.9 λ_0), resulting in a total area of about 2507 mm^2 (0.17 λ_0^2). However, due to the reduction in transverse size, the longitudinal size significantly increases, posing challenges for integration into compact mobile wireless platforms.

Recently, SW structure has been employed to minimise the entire size of substrate-integrated waveguide (SIW). It can bring extra capacitance, increasing the effective permittivity of the waveguide, and decreasing the phase velocity and guided wavelength in the waveguide. Hence, the guided wavelength inside the SW-SIW is considerably shortened according to the following equations:

$$\varepsilon_{r\_eff} = \varepsilon_r\left(\frac{h_1 + h_2}{h_1}\right) \tag{1}$$

$$v_p = \frac{c_0}{\sqrt{\mu_r \varepsilon_{r\_eff}\left(1 - f_c/f\right)}} \tag{2}$$

$$\lambda_g = \frac{v_p}{f} \tag{3}$$

where ε_{r_eff} represents the effective permittivity of the SW-SIW, v_p denotes the phase velocity, c_0 is the speed of light in free space, f_c refers to the cut-off frequency of the SW-SIW and λ_g is the guided wavelength within the SW-SIW. The detailed theorical analysis and design guidelines of the SW structure were conducted in Niembro-Martín et al. [20].

Based on this concept, many miniaturised antennas with significant size reduction have been reported. Inspired by this, the SW structure is introduced into the conventional half-wavelength $TE_{0.5,0}$ mode open waveguide to minimise the longitudinal size without disrupting its inherent performance.

The interest of the SW effect obtained with the blind via holes is shown in Figure 3b. It is clear that the electric field distribution in the cavity is similar to that of the conventional counterpart waveguide shown in Figure 3a. As a result, a significant size reduction was achieved. The longitudinal size is reduced to 69 mm, which is about 40% shorter than the traditional waveguide. Apart from length L_1, other dimension parameters remain the same. The geometrical structure, electric magnitude distributions, and surface current distributions of the traditional and SW-loaded waveguide are shown in Figure 3 for comparison. In addition, longitudinal size miniaturisation is also extracted for the design guidelines as shown in Figure 4. The size decreases with the increase of the number of blind vias since the SW effect is reinforced. Otherwise, it should be aware that when the total thickness of the cavity is fixed, higher blind via will also lead to a stronger SW effect, but results in a lower gain and more difficult impedance matching. Considering the thickness of the board available for fabrication in practice. In this paper, the height of the bind via is set to be 2 mm as an example to prove the design concept and tradeoff between the slow-wave effect and other performances. Finally, a SW-loaded $TE_{0.5,0}$ mode open waveguide with a small transverse size is designed, achieving a size reduction of 40%.

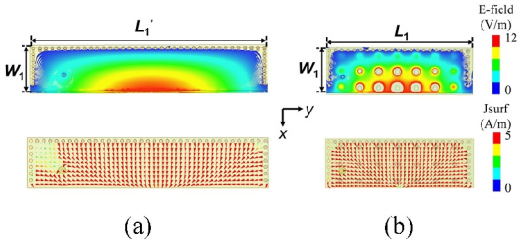

FIGURE 3 | Electric magnitude and surface current distributions of the $TE_{0.5,0}$ mode open waveguide (a) traditional type and (b) slow-wave loaded type. ($W_1 = 23$ mm, $L_1 = 69$ mm, $L_1' = 109$ mm.)

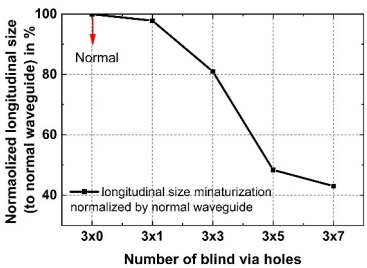

FIGURE 4 | Miniaturisation (normalised by traditional normal $TE_{0.5,0}$ waveguide dimension) of the developed SW-$TE_{0.5,0}$ waveguide.

2.3 | Operating Principle

It is well known that to achieve CP radiation, it is necessary to generate a pair of orthogonally polarised electric components. In this paper, an innovative design method that utilises the edges of the $TE_{0.5,0}$ mode open waveguide's aperture without extra size extension to realise an electric dipole working mode is proposed.

The conceptual configuration is shown in Figure 5. It is facilitated in practice by etching an open-ended slot in the top surface of the $TE_{0.5,0}$ mode open cavity. Thus, an equivalent electric dipole mode can be effectively achieved mainly by utilising the edges of the waveguide's aperture. The combination of the opening aperture radiation mode and the equivalent dipole radiation mode can ensure that the pair of orthogonal electric components has almost equal amplitude. It is worth noting that the fork-shaped slot is only for fine-tuning the phase difference, and only a vertical slot can also work.

To further illustrate the CP design concept, a half-wavelength $TE_{0.5,0}$ mode open waveguide excited by a coaxial cable is first designed. When the open waveguide works in $TE_{0.5,0}$ mode as shown in Figure 6, it can be equivalent to a magnetic dipole (M_D) that produces vertically polarised (E_θ) omnidirectional radiation at *xoz*-plane as shown in Figure 6a.

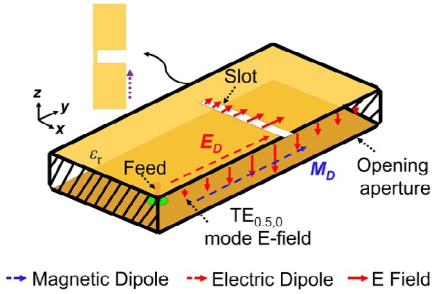

FIGURE 5 | Electric field distributions and its equivalent radiation mode of the proposed compact planar zero-ground-clearance end-fire CP antenna with complementary magnetic and electric radiators.

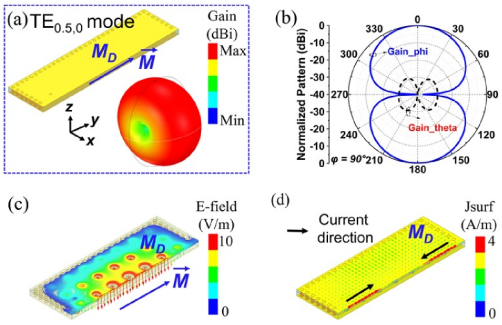

FIGURE 6 | Configuration and some simulated results of the proposed M_D. (a) $TE_{0.5,0}$ mode open waveguide with 3-D radiation pattern. (b) The normalised pattern of the $TE_{0.5,0}$ mode open waveguide in *yoz*-plane ($\varphi = 0°$) at 2.5 GHz. (c) The simulated electric field distributions on the radiating aperture and inside the waveguide at 2.5 GHz. (d) The simulated surface current distributions on the top and bottom surface of the waveguide at 2.5 GHz.

Meanwhile, its normalised pattern in the *yoz*-plane ($\varphi = 90°$) is also presented in Figure 6b for clearer understanding. In addition, Figure 6d illustrates the simulated surface current distributions for the $\lambda/2$ $TE_{0.5,0}$ mode open waveguide, it can be observed that the current distributions are relatively even, with the largest current amplitude occurring at the upper edge of the waveguide's aperture and in opposite directions.

On the other hand, as shown in Figure 7a, etching an open-ended slot in the top metallic surface of the open waveguide causes its aperture edges to generate a mode like that of a dipole antenna, providing a horizontally polarised (E_φ) radiation. This outcome occurs because, after being etched with a slot, the currents distributed along the upper and lower edge of the waveguide's aperture become uneven compared to the current distributions in Figure 6d as shown in Figure 7b. A similar effect, that is, utilising an open-ended slot on a finite ground with an end-fire horizontally polarised radiation beam, was also observed in the LP antenna [21].

To clearly demonstrate the contribution of the dipole working mode. Figure 8 shows the simulated amplitude and phase of the electric components versus θ for the $TE_{0.5,0}$ mode open waveguide without and with slot. For the waveguide without a slot, the E_θ is much larger than the E_φ and the phase difference between them is larger than 150° at $\theta = 90°$. Hence, the CP characteristics cannot be obtained in that case. After the slot in the top metallic surface of the waveguided was introduced, a dipole working mode at the edge of the waveguide's aperture is generated, and thus the amplitude of E_φ is significantly increased. In the range of $20° < \theta < 140°$, they have almost the same amplitude. Moreover, it can be observed that the dipole working mode will also significantly affect the phase of the E_φ,

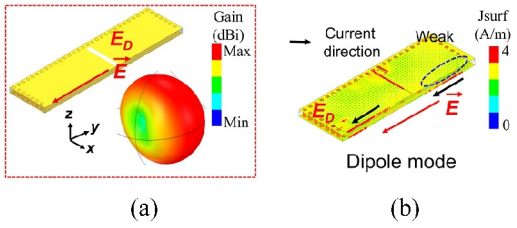

FIGURE 7 | Configuration and some simulated results of the proposed E_D. (a) Top metallic surface of the $TE_{0.5,0}$ mode open waveguide with an open-ended slot and 3-D radiation pattern. (b) The simulated surface current distributions on the top surface of the proposed CP antenna at 2.5 GHz.

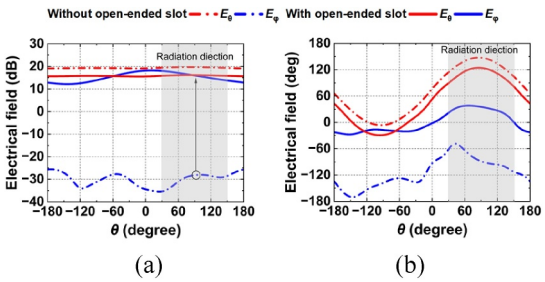

FIGURE 8 | Simulated electric components of the proposed antenna end-fire CP at 2.5 GHz (in $\varphi = 0°$). (a) Amplitude. (b) Phase.

achieving the necessary 90° phase difference in the end-fire direction for CP radiation.

Additionally, it is worth noting that in addition to the electric dipole mode, the open-end slot will also be activated. This activation helps to compensate for the Gain_phi nulls in the *yoz*-plane at $\theta = 90°$ and $\theta = 270°$ as illustrated in Figures 6b and 9b. Both M_D and E_D can realise '8'-shaped radiation patterns at *yoz*-plane ($\varphi = 90°$) as shown in Figures 6b and 9a, which have two nulls at $\theta = 90°$ and $\theta = 270°$. Thus, the synthesised radiation pattern should also exhibit two nulls at the *yoz*-plane. However, a conventional slot antenna typically features an omnidirectional horizontally polarised radiation pattern [22]. Consequently, the open-ended slot, which is perpendicular to the M_D and E_D, may provide the Gain_phi components in the *yoz*-plane to compensate for these nulls. Besides, while the open-ended slot contributes to the overall radiation, it is not dominant due to its relatively low levels.

Figure 10 shows the simulated electric vector distributions in a cut-plane in front of the antenna. The electric vector rotates in a counterclockwise direction as time increases, which indicates that the antenna radiates RHCP wave in the far-field region (note the direction of the observation).

The simulated radiation patterns at 2.5 GHz are shown in Figure 11. An end-fire RHCP radiation is achieved with a 3 dB AR beamwidth of 94° ($\varphi = 0°$) and 60° ($\theta = 90°$). The simulated gains

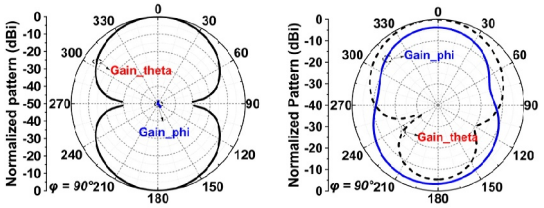

(a) (b)

FIGURE 9 | Simulated normalised patterns at 2.5 GHz in *yoz*-plane (the *yoz*-plane, $\varphi = 90°$ plane, is perpendicular to both the $\varphi = 0°$ plane [*xoz*-plane] and the $\theta = 90°$ plane [*xoy*-plane]). (a) Results of the conventional dipole located along the *y*-axis. (b) Results of the proposed compact planar zero-ground-clearance end-fire CP antenna.

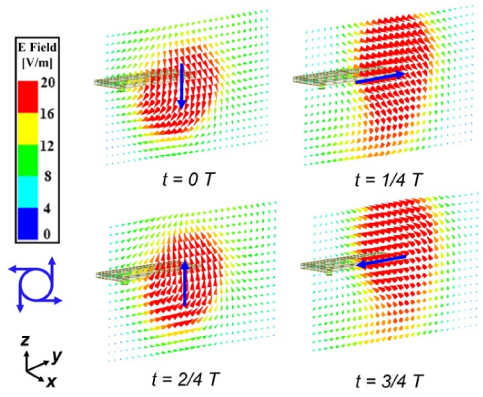

FIGURE 10 | Simulated 2.5 GHz surface vector electrical field distributions of the proposed compact planar zero-ground-clearance end-fire CP antenna at four different time phases. (T is the time period).

up to 2.53 dBic at $\theta = 60°$ but drops slightly to 2.2 dBic at $\theta = 90°$. This is due to the metal ground at the bottom of the waveguide that causes the E_D's beam to be tilted slightly upward along the $+X$ axis.

2.4 | Parametric Study

In this design, the open-ended slot plays an important role in achieving the electric dipole mode. It can affect the horizontal electric components (E_φ) and the required phase difference (PD) between the two orthogonally electric components. On the other hand, its length and position will also affect the operating frequency. Hence, the length and position of the slot should be finely tuned to meet the requirement of operational performance characteristics (CP and $|S_{11}|$). Furthermore, the antenna's operational frequency can be further optimised by changing the position of the coaxial cable.

Therefore, the variation of the antenna characteristics with some key parameters, including the length of the slot l_1 and position along the *y*-axis l_{shift} ($l_{shift} = l_2 + l_3$), and the position of the feed (l_3 and l_6), is investigated for guiding the design and optimisation of our reported antenna. These results were realised by varying one design parameter while keeping all others fixed.

First, the variation of the amplitude and phase difference between the two orthogonal electric components (E_φ and E_θ), and the $|S_{11}|$ with the slot length l_1 is illustrated in Figure 12. The change of l_1 greatly influences the PD between the two components and the $|S_{11}|$. As l_1 decreases, its amplitude and phase values will decrease and the $|S_{11}|$ values will deteriorate and shift to a higher frequency. It should be mentioned that as the l_1

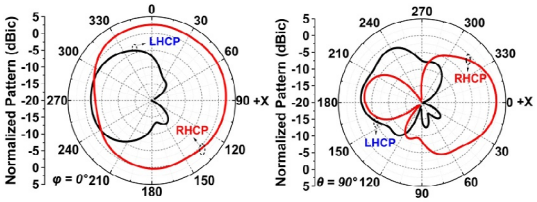

(a) (b)

FIGURE 11 | Simulated gain radiation pattern of the proposed compact planar zero-ground-clearance end-fire CP antenna at 2.5 GHz. (a) $\varphi = 0°$ and (b) $\theta = 90°$.

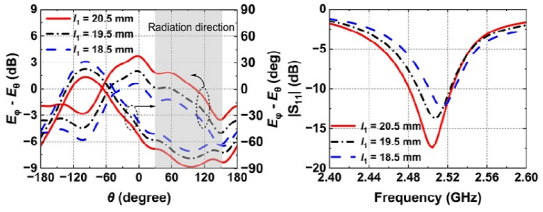

(a) (b)

FIGURE 12 | Effect of the slot length l_1 on the performance of the proposed compact zero-ground-clearance end fire CP antenna. (a) Amplitude and phase difference of the two electric components. (b) $|S_{11}|$.

decreases, the amplitude difference (AD) values at the radiation direction are still < 3 dB, but the PD values no longer satisfy the CP radiation requirement. Furthermore, when the position of the slot (l_{offset}) changes, the $|S_{11}|$ values and E_φ components are also significantly affected, as shown in Figure 13. But only have a slight influence on the PD.

Additionally, the effect of the position of the coaxial cable on the performance characteristics is also investigated in Figures 14 and 15. It can be observed that the feeding position has little impact on the CP radiation performance, but it is the key to achieving good impedance matching.

2.5 | Design Guideline

From the reported parametric studies and discussions. A general design guideline for arbitrary frequency operation was developed.

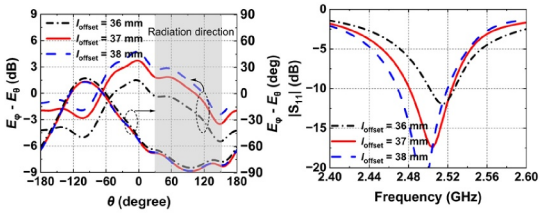

FIGURE 13 | Effect of the slot position l_{offset} ($l_{offset} = l_2 + l_3$) on the performance of the proposed compact zero-ground-clearance end fire CP antenna. (a) Amplitude and phase difference of the two electric components. (b) $|S_{11}|$.

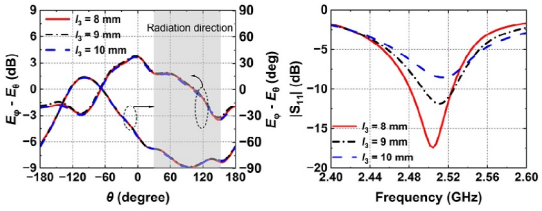

FIGURE 14 | Effect of the feeding position l_3 on the performance of the proposed compact zero-ground-clearance end-fire CP antenna. (a) Amplitude and phase difference of the two electric components. (b) $|S_{11}|$.

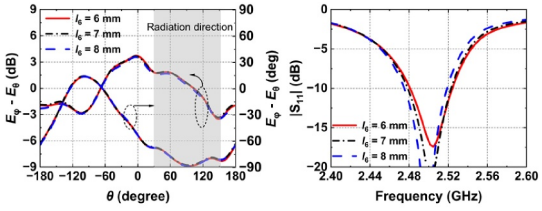

FIGURE 15 | Effect of the feeding position l_6 on the performance of the proposed compact zero-ground-clearance end-fire CP antenna. (a) Amplitude and phase difference of the two electric components. (b) $|S_{11}|$.

1. Set the operational frequency f_0.
2. Construct a conventional half-wavelength $TE_{1,0}$ mode waveguide. It involves three important parameters which are the width and length of the waveguide and dielectric constant of the substrate. These parameters are mostly selected based on the specific size requirement. Detailed guidelines for the waveguide design can be found in Lin and Ziolkowski [19].
3. Integrated the slow-wave structure. Incorporate the slow-wave structure into the designed $TE_{1,0}$ mode waveguide. Then, construct a half wavelength $TE_{0.5,0}$ mode open waveguide. The detailed design method for a slow-wave waveguide has been presented in Niembro-Martín et al. [20]. Note that a strong slow-wave effect will significantly reduce the gain and other performance. Therefore, there is a trade-off between size and performance.
4. Design the open-ended slot. It is the key to obtaining the CP radiation. Its length and position should be finely tuned according to the simulated results as illustrated and discussed in Figures 12 and 13. In addition, the direction of polarisation is mainly related to the position of the feed, the antenna can radiate RHCP when the slot is on the right side of the feed. When it is on the left side, it can radiate LHCP.
5. Optimise the feeding position. Adjust the position of the feeding part to ensure the antenna operates at the frequency f_0.

By following the abovementioned steps, a planar end-fire CP antenna with zero ground clearance and compact size is obtained.

3 | Fabrication and Experimental Results

To verify the design concept described above, a compact planar end-fire CP antenna with an integrated SW structure was fabricated, assembled and measured. Figure 16a shows the fabricated antenna components before assembly. Photographs of

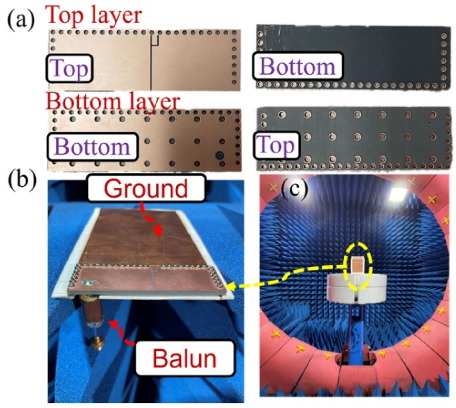

FIGURE 16 | Fabricated prototype of the proposed compact planar zero-ground-clearance end-fire CP antenna. (a) Top and bottom views of each substrate before assembly. (b) Side view of the assembled antenna mounted on a copper ground. (c) Measurement environment.

the assembled antenna are presented in Figure 16b. The antenna is fed by a 50 Ω coaxial line. To suppress the current leakage on the outer conductor of the long coaxial, a classical sleeve balun (24 mm) was employed in the measurement and thus ensure the accuracy of the measurement results of far-field radiation. Because this prototype is only fabricated to prove the design concept, instead of using the expensive stack-up processing technology, metal screws were used to secure the two PCB boards. The impact on the antenna performance is also analysed. Additionally, the metal ground (70 mm × 150 mm) was used to mimic the mainboard of mobile devices, and the antenna was mounted on one side of the ground.

The simulated and measured reflection coefficients and realised gain values as functions of source frequency are reported in Figure 17a. The measured $|S_{11}|$ values are slightly wider than simulated values (0.7%), with the resonant frequency point shifted towards higher frequencies (20 MHz). However, the trend of the measured results aligns well with the simulated results. The main reasons for this phenomenon may be due to parasitic parameters generated during the soldering of the feeding cable as well as the assembly stage. The measure 10 dB impedance bandwidth was 2.8%, covering 2.48–2.55 GHz. The measure and simulated peak realised gain values at $+X$-direction ($\varphi = 0°$ and $\theta = 90°$) are 2.05 and 1.9 dBic, respectively. The measured and simulated AR values as functions of source frequency at the $+X$-direction are plotted in Figure 17b. The measured 3 dB AR bandwidth reaches 2.7% from 2.495 to 2.562 GHz (2.8%, from 2.45 to 2.52 GHz). Therefore, the measured overlapped bandwidth is 2.8% ($|S_{11}| < -10$ dB and AR < 3 dB). Notably, all the measured results were slightly shifted to a higher frequency compared with the simulated ones as shown in Figure 17. To analyse the reason for this phenomenon, the variation of the reflection coefficients and AR values with the Gap (refers to the gap between two layers of PCBs) is plotted Figure 18. All other parameters are kept fixed. It can be observed that when the Gap is slightly increased, both the reflection coefficients and AR values are shifted towards the higher frequencies. At the same time, the AR values deteriorate, but good AR performance can be obtained by slightly tuning the length of the slot.

Figure 19 shows the measured and simulated normalised realised gain pattern and AR beam width at two vertical planes. The measured and simulated results coincide well with each other. The Co-polarisation (RHCP) of the designed antenna is towards the $+X$-direction (end-fire direction). The simulated AR beamwidths in $\varphi = 0°$ and $\theta = 90°$ planes are 94° and 62°, while the measured results are 70° and 50°, respectively. Assembly and test tolerances may be responsible for the differences in beamwidth and ripple between measured and simulated radiation performance.

A comparison with the reported planar end-fire CP antennas is summarised in Table 1. It verifies that our developed antenna achieves zero ground clearance, wider overlapped bandwidth and small transverse size, especially when taking into account its longitudinal dimension. More importantly, about 40% of size miniaturisation is realised by introducing a SW structure. In fact, the longitudinal size depends strongly on the transverse size of the half-wavelength $TE_{0.5,0}$ mode resonant waveguide. The longitudinal size can be significantly reduced by slightly increasing the transverse size. In this case, we only illustrate the design concept of the work. It has the potential to achieve a small footprint. Of course, it also can be designed according to the specific requirements. Moreover, compared with the existing designs, our proposed design also considered the effect of the

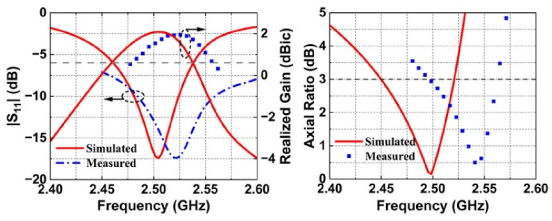

(a) (b)

FIGURE 17 | Simulated and measured results as functions of source frequency for the proposed compact planar zero-ground-clearance end-fire CP antenna. (a) $|S_{11}|$ and realised gain. (b) Axial ratio values at $\varphi = 0°$ and $\theta = 90°$.

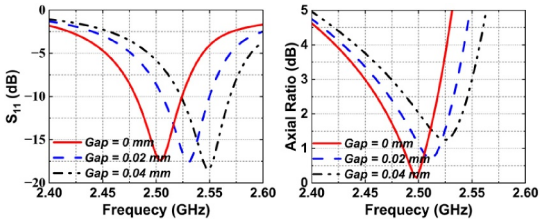

(a) (b)

FIGURE 18 | Effect of the gap between top and bottom substrate on the performance characteristics of the compact planar zero-ground-clearance end-fire CP antenna. (a) $|S_{11}|$. (b) Axial ratio values.

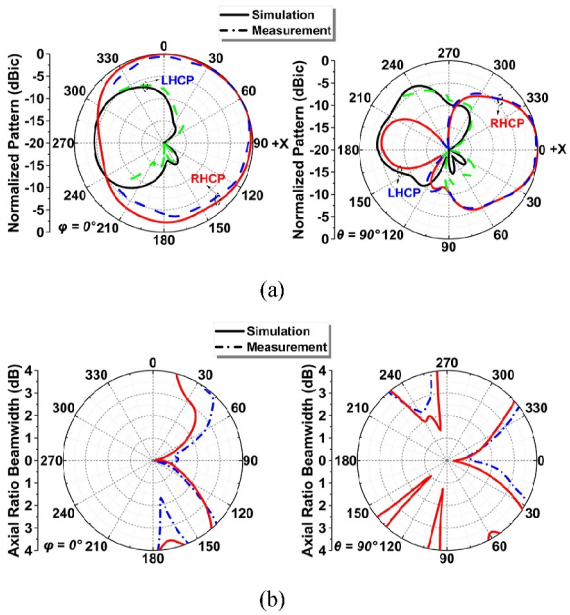

(a)

(b)

FIGURE 19 | Simulated and measured far-field results at two vertical planes, $\varphi = 0°$ and $\theta = 90°$, for the proposed compact planar zero-ground-clearance end-fire CP antenna (2.5 GHz in simulation and 2.53 GHz in experiment). (a) Normalised realised gain pattern. (b) Axial ratio beam width.

TABLE 1 | Comparison of the proposed antenna with other works.

Refs.	Structure	Overlapped bandwidth	Ground clearance (λ_0)	Size (λ_0^2)
[9]	Cavity + loop	2.4%	0.42	0.7 × 0.6[a]
[10]	Cavity + dipole	1.9%	0.49	0.73 × 0.65[a]
[13]	Cavity + dipole	3.5%	0.17	0.6 × 0.32[a]
[14]	CMPA + slot	1.2%	0.25	0.49 × 0.25[a]
This work	SW_SIW + slot	2.7%	0	0.57 × 0.19[a]

[a]Transverse size.

large metallic ground of practical devices. Considering these attractive features, it would be desirable for end-user communication with a constrained volume.

4 | Conclusion

In this paper, a planar end-fire CP antenna without ground clearance is successfully implemented by sharing the vertically and horizontally polarised radiators on a $\lambda/2$ $TE_{0.5,0}$ mode open waveguide. The miniaturised method, design concept and operating mechanism were presented. The method of designing an open-ended slot in the top surface of the waveguide to achieve the horizontal polarisation and the required 90-phase difference was explained. Parameter studies of the key variables have been carefully discussed to establish engineering design guidelines. A prototype was fabricated and measured. The measured results show a reasonable agreement with the simulated ones. In summary, the developed planar SW-loaded end-fire CP features zero ground clearance, compact size, and a simple configuration. It provides a feasible example of the total integration with the substrate board. Therefore, the antenna can be a candidate for satellite communications, RFID and many other wireless scenarios.

Author Contributions

Wei Lin and Chow-Yen-Desmond Sim contributed to the conceptualisation and methodology design of the paper. Huacheng Li and Wei Lin conceived and designed the experiments. Huacheng Li wrote the paper. Wei Lin revised and improved the quality of the paper.

Conflicts of Interest

The authors declare no conflicts of interest.

Data Availability Statement

The data that support the findings of this study are openly available.

References

1. X. Teng, Y. Hou, S. Wang, N. Yan, Y. Luo, and K. Ma, "Single-Conductor Planar Ladder Endfire Antenna," *IEEE Antennas and Wireless Propagation Letters* 23, no. 7 (2024): 1986–1990, https://doi.org/10.1109/LAWP.2024.3376073.

2. S. Gao, Q. Luo, and F. Zhu, *Circularly Polarized Antennas* (John Wiley & Sons, 2014).

3. Z. Cao, L. Chang, Y. Li, K. Wei, and Z. Zhang, "Compact Mobile Terminal Antenna With Endfire Circularly Polarized Beam for Satellite Communications," *IEEE Transactions on Antennas and Propagation* 71, no. 12 (2023): 9980–9985, https://doi.org/10.1109/TAP.2023.3325204.

4. W.-H. Zhang, P. Cheong, W. J. Lu, and K. W. Tam, "Planar Endfire Circularly Polarized Antenna for Low Profile Handheld RFID Reader," *IEEE Journal of Radio Frequency Identification* 2, no. 1 (2018): 15–22, https://doi.org/10.1109/JRFID.2018.2817570.

5. P. F. Hu, Y. M. Pan, S. Zheng, and B. J. Hu, "The Design of Miniaturized Planar Endfire Antenna With Enhanced Front-to-Back Ratio," *IEEE Transactions on Antennas and Propagation* 68, no. 10 (2020): 7190–7195, https://doi.org/10.1109/TAP.2020.2977816.

6. Z. Chen and Z. Shen, "Planar Helical Antenna of Circular Polarization," *IEEE Transactions on Antennas and Propagation* 63, no. 10 (2015): 4315–4325, https://doi.org/10.1109/TAP.2015.2463746.

7. S. Ge, Q. Zhang, A. K. Rashid, Y. Zhang, M. Yu, and R. Murch, "Low-Profile High-Gain Endfire Antenna With Circular Polarization," *IEEE Transactions on Antennas and Propagation* 70, no. 8 (2022): 7181–7186, https://doi.org/10.1109/TAP.2022.3164216.

8. Q. Wu, J. Hirokawa, J. Yin, C. Yu, H. Wang, and W. Hong, "Millimeter Wave Multibeam Endfire Dual-Circularly Polarized Antenna Array for 5G Wireless Applications," *Transactions on Antennas and Propagation* 66, no. 9 (2018): 4930–4935, https://doi.org/10.1109/TAP.2018.2851667.

9. W.-J. Lu, J. W. Shi, K. F. Tong, and H. B. Zhu, "Planar Endfire Circularly Polarized Antenna Using Combined Magnetic Dipoles," *IEEE Antennas and Wireless Propagation Letters* 14 (2015): 1263–1266, https://doi.org/10.1109/LAWP.2015.2401576.

10. W.-H. Zhang, W.-J. Lu, and K.-W. Tam, "A Planar End-Fire Circularly Polarized Complementary Antenna With Beam in Parallel With Its Plane," *IEEE Transactions on Antennas and Propagation* 64, no. 3 (2016): 1146–1152, https://doi.org/10.1109/TAP.2016.2518204.

11. M. You, W. J. Lu, B. Xue, L. Zhu, and H. B. Zhu, "A Novel Planar Endfire Circularly Polarized Antenna With Wide Axial-Ratio Beamwidth and Wide Impedance Bandwidth," *IEEE Transactions on Antennas and Propagation* 64, no. 10 (2016): 4554–4559, https://doi.org/10.1109/TAP.2016.2593929.

12. L. Wang, Y.-C. Jiao, and Z. Weng, "Novel Dual-Band Circularly Polarized Planar Endfire Antenna With Enhanced Front-to-Back Ratios," *IEEE Transactions on Antennas and Propagation* 70, no. 2 (2022): 969–976, https://doi.org/10.1109/TAP.2021.3111160.

13. M. Ye, X.-R. Li, and Q.-X. Chu, "Single-Layer Circularly Polarized Antenna With Fan-Beam Endfire Radiation," *IEEE Antennas and Wireless Propagation Letters* 16 (2017): 20–23, https://doi.org/10.1109/LAWP.2016.2552490.

14. L. Guo, "Compact Wide-Beam Circularly Polarized End-Fire Antenna Combining Ground Radiation Mode and Vertically Polarized Mode," *IEEE Transactions on Antennas and Propagation* 70, no. 11 (2022): 10218–10225, https://doi.org/10.1109/TAP.2022.3195451.

15. L. Sun and H. Wang, "Circularly-Polarized Antenna Design in Mobile Phones by the Combination of Common and Differential Modes," in *2024 IEEE MTT-S International Wireless Symposium (IWS)* (2024), 1–3, https://doi.org/10.1109/IWS61525.2024.10713522.

16. W.-J. Lu, K. Wang, S. S. Gu, L. Zhu, and H. B. Zhu, "Directivity Enhancement of Planar Endfire Circularly Polarized Antenna Using V-Shaped 1.5-Wavelength Dipoles," *IEEE Antennas and Wireless Propagation Letters* 18, no. 7 (2019): 1420–1423, https://doi.org/10.1109/LAWP.2019.2918505.

17. Y. Yin and K. Wu, "Endfire Circularly-Polarized Antipodal Linearly Tapered Slot Antenna Fed by Slotted Width-Tapered SIW," *IEEE Transactions on Antennas and Propagation* 70, no. 4 (2022): 2411–2421, https://doi.org/10.1109/TAP.2021.3109159.

18. J. Zhang, M. O. Akinsolu, B. Liu, and S. Zhang, "Design of Zero Clearance SIW Endfire Antenna Array Using Machine Learning-Assisted Optimization," *IEEE Transactions on Antennas and Propagation* 70, no. 5 (2022): 3858–3863, https://doi.org/10.1109/TAP.2021.3137500.

19. W. Lin and R. W. Ziolkowski, "High-Directivity, Compact, Omnidirectional Horizontally Polarized Antenna Array," *IEEE Transactions on Antennas and Propagation* 68, no. 8 (2020): 6049–6058, https://doi.org/10.1109/TAP.2020.2983786.

20. A. Niembro-Martín, V. Nasserddine, E. Pistono, et al., "Slow-Wave Substrate Integrated Waveguide," *IEEE Transactions on Microwave Theory and Techniques* 62, no. 8 (2014): 1625–1633, https://doi.org/10.1109/TMTT.2014.2328974.

21. Y. Xu, N. Liu, and L. Zhu, "Wideband Microstrip-Fed Slot Antenna With End-Fire Radiation Under Dual-Resonant Modes," *International Journal of RF and Microwave Computer-Aided Engineering* 30, no. 12 (2020): 1–11, https://doi.org/10.1002/mmce.22458.

22. C. A. Balanis, *Antenna Theory: Analysis and Design*, 3rd ed. (Wiley, 2005).